Magnetic Resonance in Medicine 50:154–163 (2003)

Real-Time Imaging of Two-Dimensional Cardiac Strain Using a Harmonic Phase Magnetic Resonance Imaging (HARP-MRI) Pulse Sequence

Smita Sampath,[1] J. Andrew Derbyshire,[2] Ergin Atalar,[3] Nael F. Osman,[3] and Jerry L. Prince[1,3*]

The harmonic phase (HARP) method provides automatic and rapid analysis of tagged magnetic resonance (MR) images for quantification and visualization of myocardial strain. In this article, the development and implementation of a pulse sequence that acquires HARP images in real time are described. In this pulse sequence, a CINE sequence of images with 1-1 spatial modulation of magnetization (SPAMM) tags are acquired during each cardiac cycle, alternating between vertical and horizontal tags in successive heartbeats. An incrementing train of imaging RF flip angles is used to compensate for the decay of the harmonic peaks due to both T_1 relaxation and the applied imaging pulses. The magnitude images displaying coarse anatomy are automatically reconstructed and displayed in real time after each heartbeat. HARP strain images are generated offline at a rate of four images per second; real-time processing should be possible with faster algorithms or computers. A comparison of myocardial contractility in non-breath-hold and breath-hold experiments in normal humans is presented. Magn Reson Med 50:154–163, 2003. © 2003 Wiley-Liss, Inc.

Key words: real-time imaging; magnetic resonance tagging; harmonic phase; cardiac motion; myocardial strain; FastHARP

The ability to rapidly detect the onset of an ischemic event is critical to patient safety during cardiac stress exams. Currently, 2D and 3D cardiac function can be quantified using several magnetic resonance (MR) techniques—e.g., phase contrast (PC) velocity imaging (1–4), stimulated echo (SE) (5,6), and tagging (7–15). However, delayed and unreliable detection of ischemia has limited the use of MRI in cardiac stress exams.

In PC velocity imaging, strain-rate tensors are obtained by computing spatial derivatives of the phase (2,4). Strains are computed by integrating the velocity data and determining the trajectories of the displacement (1,3).

In SE techniques (5,6), the phase is proportional to the displacement, and strain measures are obtained by computing spatial phase gradients. Both PC and SE techniques provide functional information at high spatial resolutions, but generally require lengthy data acquisition protocols.

MR tagging spatially modulates the longitudinal magnetization at end-diastole, creating tag patterns that when imaged reveal the underlying motion of the heart (7).

Clinical adoption of tagged MRI has been delayed because of its lengthy image acquisition times and tedious image analysis requirements. For example, currently it may take eight to 20 heartbeats over a breath-hold to acquire a CINE sequence of tagged images, and 5–10 min to process these images with manual assistance (10,11,15,16).

The harmonic phase (HARP) method is a relatively new technique that provides automatic postprocessing methods for strain analysis (12−14). In the Fourier domain, spatial modulation of magnetization (SPAMM) tagged MR data (8,9) has several spectral peaks. HARP uses the fact that the phase of the image corresponding to an off-origin spectral peak is directly related to the tissue motion. Spatial derivatives of HARP are computed at each pixel to obtain strain measures. The required computations are fast and automated, and provide displacement or strain maps from the acquired tagged data in seconds (12–14). It is current practice to acquire conventional high-resolution tagged images (usually higher-order SPAMM), and to use a bandpass filter to extract the desired spectral peak for HARP postprocessing.

In this work we present a pulse sequence called HARP-MRI, which exploits the fact that only two spectral peaks are sufficient for the computation of 2D-motion information. The HARP-MRI pulse sequence acquires multiframe HARP images in a single heartbeat for a given tag orientation. Data acquired in only two heartbeats are used to compute in-plane quantities describing myocardial deformation for a single slice, thereby reducing the required breath-hold interval. To demonstrate and compare the performance of HARP-MRI, we scanned six normal human volunteers, acquiring non-breath-hold HARP-MRI data, breath-hold HARP-MRI data, and breath-hold conventional tagged MRI data.

BACKGROUND

Figure 1a shows the Fourier transform of a 1-1 SPAMM tagged MR image. This image has three spectral peaks: a DC peak centered at the origin of the Fourier space, and two harmonic peaks centered at the tag pattern frequencies (both positive and negative). The harmonic peaks result from the modulation of the longitudinal magnetization with the sinusoidal tag pattern.

[1]Image Analysis and Communications Laboratory, Department of Electrical and Computer Engineering, Johns Hopkins University, Baltimore, Maryland.

[2]Laboratory of Cardiac Energetics, NHLBI, Bethesda, Maryland.

[3]Department of Radiology, Johns Hopkins University, Baltimore, Maryland.

Grant sponsor: National Heart, Lung, and Blood Institute; Grant number: R01HL47405.

Drs. Prince and Osman are founders of and own stock in Diagnosoft, Inc., a company that seeks to license the HARP technology. The terms of this arrangement are being managed by the Johns Hopkins University in accordance with its conflict of interest policies.

*Correspondence to: Jerry L. Prince, Image Analysis and Communications Laboratory, Department of Electrical and Computer Engineering, 307 Barton Hall, Baltimore, MD 21218. E-mail: prince@jhu.edu

Received 19 October 2001; revised 6 March 2003; accepted 8 March 2003.

DOI 10.1002/mrm.10509

Published online in Wiley InterScience (www.interscience.wiley.com).

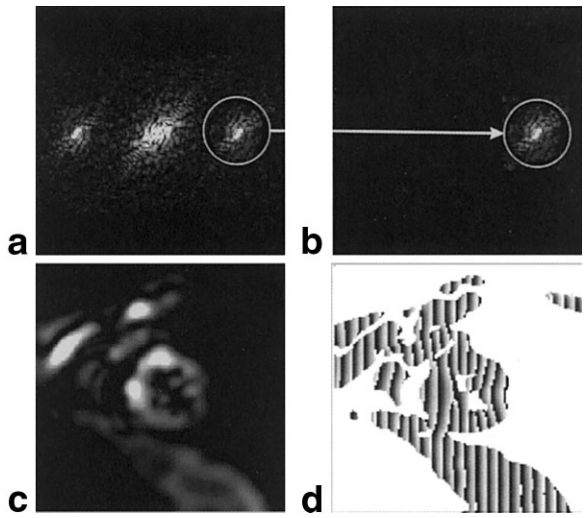

FIG. 1. (**a**) The Fourier transform of a 1-1 SPAMM image and (**b**) an isolated harmonic peak. (**c**) Harmonic magnitude and (**d**) HARP images obtained by reconstructing **b**. Both **c** and **d** are masked for improved visualization.

A harmonic image can be constructed by bandpass filtering one of the off-centered harmonic peaks while padding the surrounding space with zeros (as illustrated in Fig. 1b), and then taking the inverse Fourier transform. The resulting image can be expressed as (12−14):

$$I(\mathbf{p}, t) = D(\mathbf{p}, t)e^{j\phi(\mathbf{p}, t)}, \quad [1]$$

where the vector $\mathbf{p} = (x,y)$ is the spatial position of a pixel in the image plane, and t is the time that has elapsed after tag application. The magnitude image $D(\mathbf{p},t)$ is proportional to the magnitude of the transverse magnetization at point $\mathbf{p}$ and time t (see Fig. 1c), and the phase image $\phi(\mathbf{p},t)$ is related to the displacement in the motion-encoded direction (which is perpendicular to the direction of the tag planes) at position $\mathbf{p}$ and time t. We can compute a HARP image $a(\mathbf{p},t) = \angle I(\mathbf{p},t)$ from the observed harmonic image, yielding a phase-wrapped version of the underlying true phase with values ranging from $-\pi$ to $+\pi$ (see Fig. 1d). Tissue displacement in the direction perpendicular to the tag orientation is reflected as a local change in the phase of the harmonic image, and the phase contours in these harmonic images deform similarly to tag lines (13). It has previously been shown that harmonic images can be used to obtain measures of displacement and strain (12–14) (Appendix A) and to generate synthetically tagged images (17) (Appendix B).

METHODS

HARP-MRI Pulse Sequence

All experiments were conducted on a 1.5T Signa CV/i whole-body MR system (GE Medical Systems, Waukesha, WI) equipped with 40 mT/m imaging gradients with slew rates up to 150 mT/m-ms. A gated, multiphase, interleaved, gradient-echo EPI pulse program was modified to provide a real-time HARP imaging pulse sequence, termed HARP-MRI.

A complete HARP-MRI acquisition requires two heartbeats (18). The sequence timing diagram in Fig. 2 shows the HARP-MRI pulse sequence over one heartbeat. During the first heartbeat, vertical 1-1 SPAMM tags are generated at end-diastole triggered by the R wave of the ECG by applying two 90° RF pulses (A and C), separated by a tagging gradient (B) in the x direction. Crusher gradient pulses are then applied to spoil residual magnetization in the transverse plane. A tag separation of 8 mm is typically used.

Once the tags are created, acquisition of a small region in *k-space* around the selected spectral peak begins. Radiofrequency (RF) imaging pulses (D) with an incrementing train of flip angles α_i that bear a specific relation with each other (19,20) are applied to equalize the signal strength (magnitude) in each cardiac phase by compensating for the tag fading caused by longitudinal relaxation and imaging pulses. To maximize the signal strength per cardiac phase, a program is run before the scan to determine the optimal final flip angle (typically 14–18°). A plot of the HARP image contrast, defined as the ratio of the magnitude of the harmonic image $D(\mathbf{p},t)$ to the steady-state magnetization, is generated (see Fig. 3). The curves are generated for combinations of final flip angles in the range of 1–50° and percentage of the cardiac cycle not imaged in the range of 1–50%. The final flip angle is selected as the peak of the curve corresponding to the percentage of the cardiac cycle not imaged (as determined by the subject heart rate and desired fraction of the heartbeat to image). The choice of the myocardial tissue T_1 value used in the computation of the HARP image contrast is important. It can be shown that overestimation (resp. underestimation) of the actual T_1 value can result in dimming (resp. brightening) in the magnitude in each subsequent TR acquisition. We used T_1 = 850 ms in our computations because this yielded images with visually uniform signal strength. For example, in one volunteer, we found a decrease in the signal-to-noise ratio (SNR) of the harmonic magnitude images from 30 dB to 19 dB while imaging 60% of the cardiac cycle, and using a constant imaging flip angle of 20°. Using the incrementing train of imaging flip angles, with a T_1 of 850 ms and an optimized final flip angle of 14°, the SNR varied between 25 dB and 27 dB over all the cardiac phases imaged.

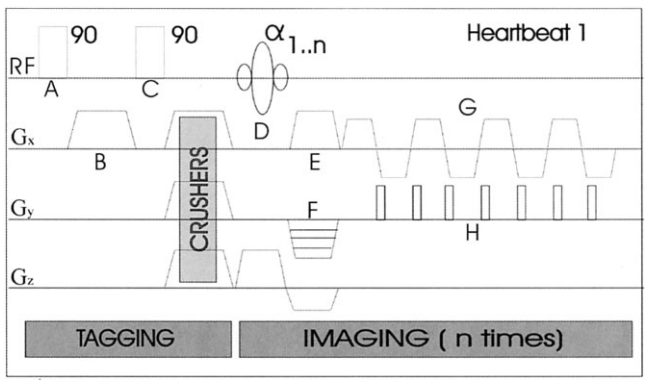

FIG. 2. A timing diagram of the HARP-MRI pulse sequence.

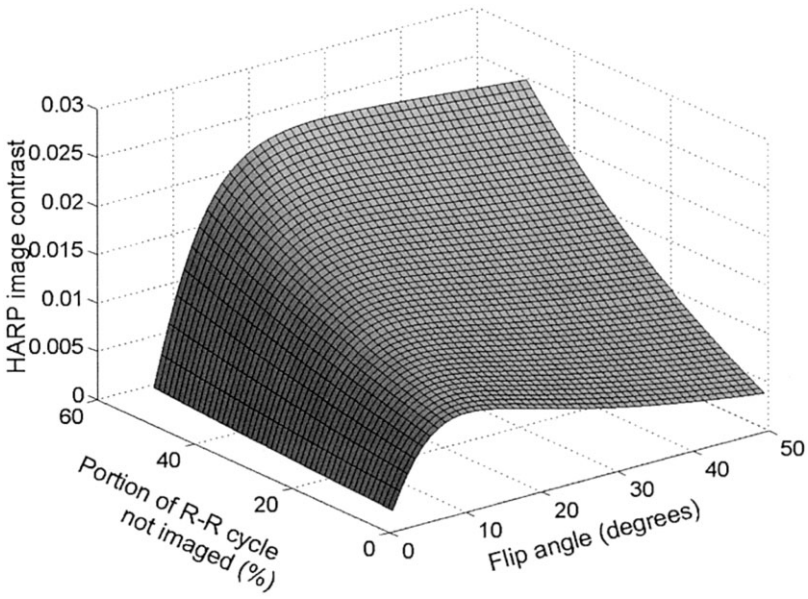

FIG. 3. Plot of the HARP image contrast vs. the percentage of the cardiac cycle not imaged, and the final imaging flip angle in degrees. Heart rate = 60 bpm, TR = 9.7 ms, and T_1 = 850 ms.

To shift the center of the acquisition window to the center of the harmonic peak, the read dephaser gradient (E) and the phase-encoding table (F) areas are modified (Fig. 2). A gradient-echo EPI sequence (G) with four interleaved shots is then used to acquire a 32 × 32 matrix in *k*-space centered on the spectral peak. A bottom-up scheme is used to traverse the *k*-space during each shot with an echo-train of length 8. A receiver bandwidth of 62.5 kHz was found to be an optimal compromise between acquisition time and SNR for 32 readout samples for the given slew rate. These parameters result in a TR of 9.7 ms. The effective TE used was 2 ms.

Depending on the heart rate, seven to 20 images can be acquired in one heartbeat, with a 40-ms total acquisition time for each image. The second heartbeat is used to acquire HARP images with an orthogonal tag orientation. To accomplish this, the frequency (G_x) and phase (G_y) directions are swapped in the second heartbeat.

We refer to the two-heartbeat HARP-MRI acquisition as the "single-shot" mode. HARP-MRI can also be run in a "continuous" mode, in which HARP images are continuously acquired with tags alternating between vertical and horizontal orientations in successive heartbeats. In this mode, HARP strain (or displacement) images can be obtained every heartbeat by processing the images acquired during the preceding two heartbeats.

Multicoil Data Combination

A receive-only, cardiac, four-channel, phased-array receiver coil (GE Medical Systems, Waukesha, WI) was used to acquire the HARP data. Each coil *i* has a spatially localized complex sensitivity profile that alters the underlying magnitude and phase of the image. Hence, the harmonic image obtained from coil *i* can be expressed as

$$I_i(\mathbf{p},t) = D(\mathbf{p},t)e^{j\phi(\mathbf{p},t)}\, M_i(\mathbf{p})e^{j\theta_i(\mathbf{p})}. \quad [2]$$

Artifact-free phase reconstruction relies on the accurate measurement of the individual complex sensitivity profiles for each of the four coils, which is a time-consuming process. In lieu of this, the combined magnitude image was obtained using the standard sum-of-squares method, which can be expressed as follows:

$$D_{comb}(\mathbf{p},t) = \sqrt{\Sigma_{i=1}^{4}|I_i(\mathbf{p},t)|^2}. \quad [3]$$

To obtain a combined phase image, a reference scan was acquired just prior to every main scan. The reference scan was identical to the main HARP acquisition sequence, except that the acquisition window was centered on the DC peak rather than the harmonic peak. The reference scan required two heartbeats (one for each tagged direction), during which multiframe images were acquired. The DC images obtained by reconstructing these datasets for each coil *i* can be characterized as follows:

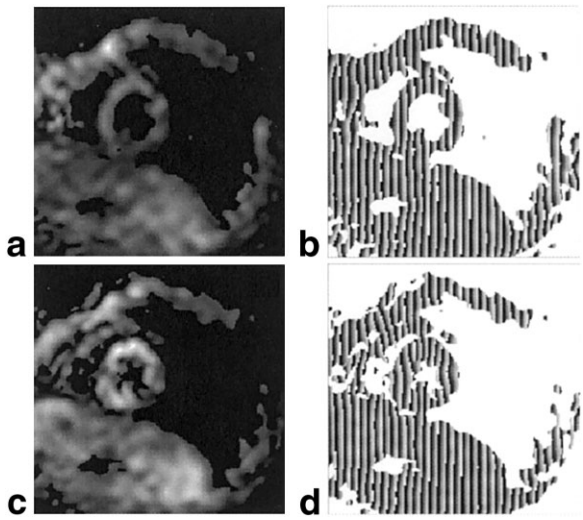

FIG. 4. Harmonic magnitude images and HARP images obtained using the HARP-MRI sequence with a two-heartbeat breath-hold at (**a** and **b**) end-diastole and (**c** and **d**) end-systole.

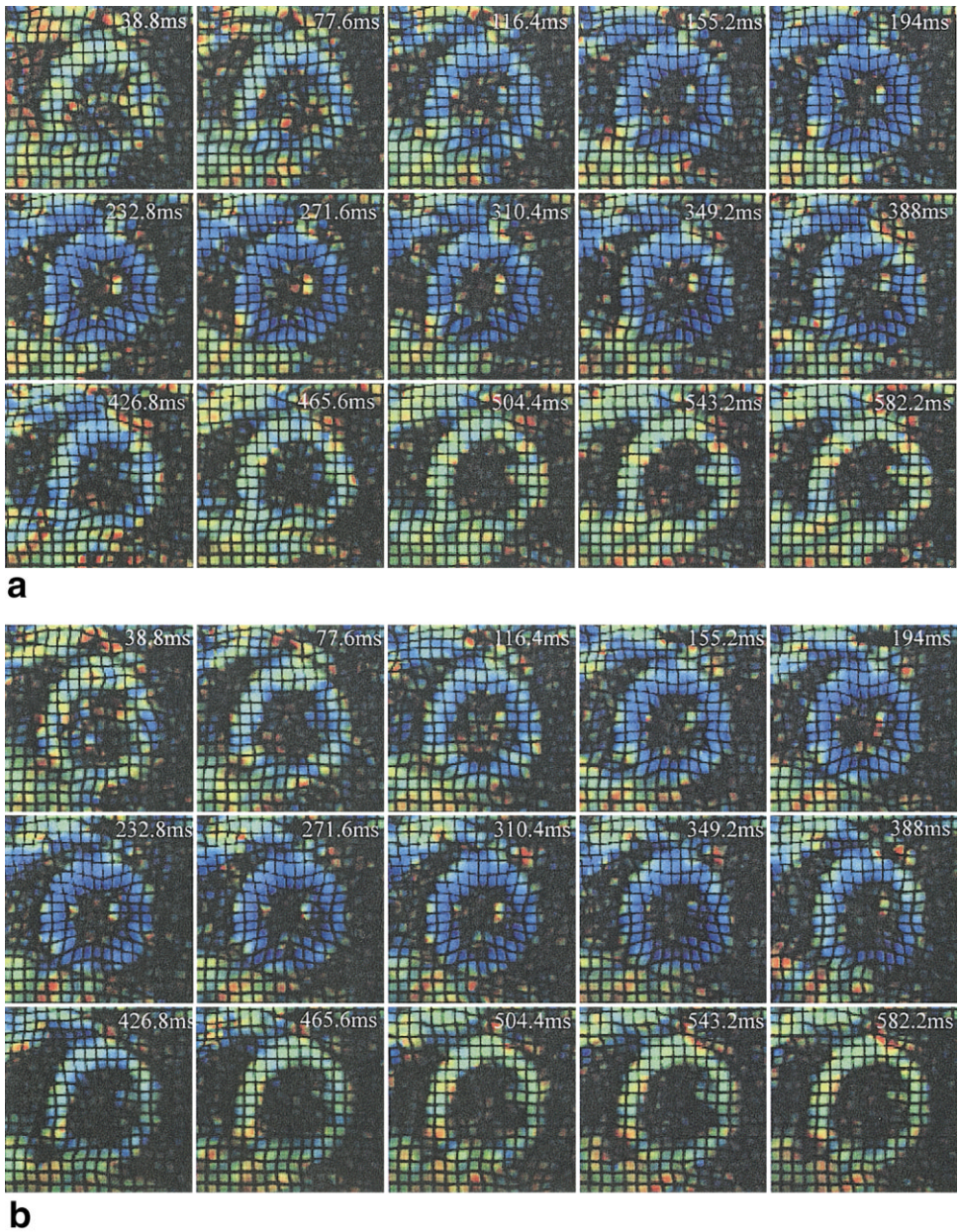

FIG. 5. Eulerian circumferential strain maps displayed on synthetic tagged image sequences. (**a)** A two-heartbeat breath-hold HARP-MRI scan. (**b)** A non-breath-hold HARP-MRI scan. (**c)** High-resolution, "standard" tagged data acquisition requiring two breath-holds of 12 heartbeats each.

$$I_i^{dc}(\mathbf{p},t) = D^{dc}(\mathbf{p},t)M_i(\mathbf{p})e^{j\theta_i(\mathbf{p})}. \quad [4]$$

Here, there is no motion-related phase term, so it becomes clear that the DC images acquired at any given cardiac frame and a given tagged direction can be used as a phase reference for the harmonic image acquired during the same cardiac frame and tag direction.

The phases were then combined using an extension of the corrected phase difference method (21), which is mathematically described as

$$\phi_{comb}(\mathbf{p},t) = arg\{\sum_{i=1}^{4} I_i(\mathbf{p},t)^* I_i^{dc}(\mathbf{p},t)\}. \quad [5]$$

Using the combined magnitude and phase terms from Eqs. [3] and [5], respectively, the final image obtained after combining the individual coil images can be expressed as

$$I_{comb}(\mathbf{p},t) = D_{comb}(\mathbf{p},t)e^{j\phi_{comb}(\mathbf{p},t)}. \quad [6]$$

Normal Volunteer Experiments

The imaging experiments in human subjects were approved by the Institutional Review Board of Johns Hopkins University, and informed consent was obtained from all subjects. The data presented here were obtained from six normal human volunteers (mean age 30 ± 8 years) with no prior history of cardiac disease or chest pain. For each volunteer, an oblique, short-axis, 10-mm-thick mid-ventricular slice of the left ventricle was prescribed with a field of view (FOV) in the range of 28–32 cm.

For all six volunteers, two kinds of HARP-MRI datasets (non-breath-hold and breath-hold) were acquired. A reference scan was run to acquire the DC peaks, which were used as the phase reference images during subsequent phase-sensitive reconstruction. This was followed by a

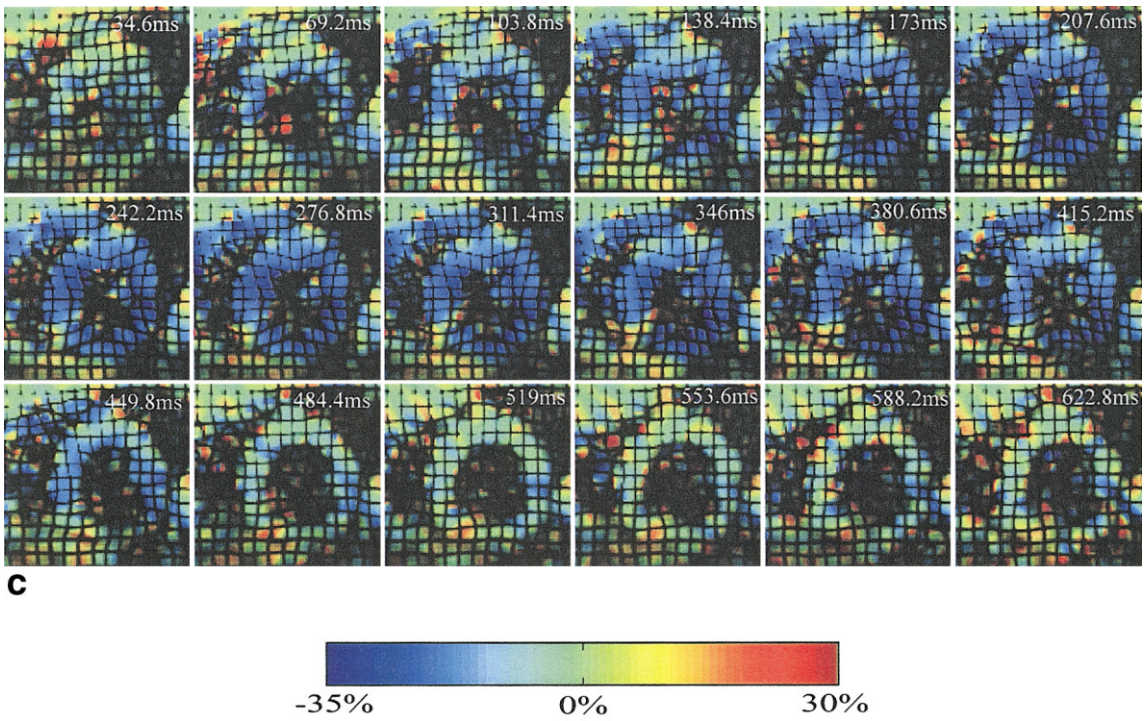

FIG. 5. Continued.

breath-hold scan lasting two heartbeats. The experiment was then repeated with the volunteer breathing freely during the scan. The free-breathing scan lasted about 10 heartbeats, but only data from the last two consecutive heartbeats were analyzed. The magnitude images displaying coarse anatomy were automatically reconstructed and displayed in real time after each heartbeat on a nearby workstation (22–24).

Currently, HARP strain images are computed offline. The raw data obtained from each coil were reconstructed to size 256 × 256 by zero-filling, and the magnitudes and phases were combined using Eqs. [3] and [5], respectively, to produce a combined image using Eq. [6].

In three of the volunteer studies, conventional 1-1 SPAMM tagged, gated, segmented *k*-space, interleaved gradient-echo EPI images were also obtained. This sequence was used to acquire 15–20 cardiac phases of the same slice using 1-1 SPAMM tagging. All three spectral peaks were acquired. These images were acquired over two breath-holds, one for each tag direction, each lasting 12 heartbeats. The size of the image matrix was 256 × 192, with a FOV in the range of 28–32 cm. During each heartbeat, two interleaved shots were acquired, with each shot comprising of an echo train of length 8. A receiver bandwidth of ±125 kHz was used, resulting in a TR of 17.32 ms. To use this data in HARP processing, two spectral peaks (one horizontal and one vertical) were isolated using bandpass filtering.

The three sets of acquired images were then processed independently using the HARP software to generate two different measures of strain: Eulerian and Lagrangian. Eulerian circumferential strain maps, wherein the rate of deformation at fixed points in space is computed regard-

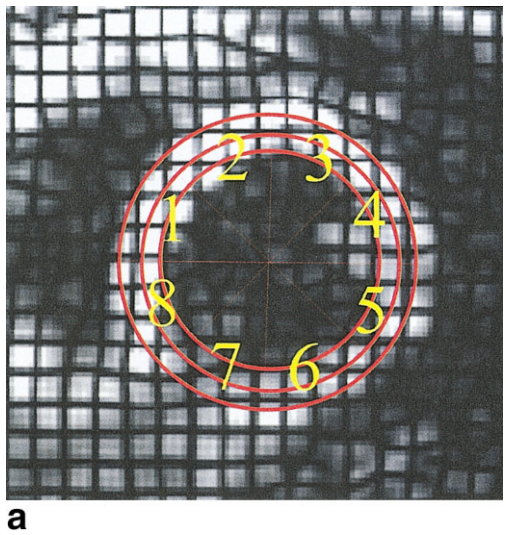

FIG. 6. **a:** Circular grid superimposed on the left ventricular wall depicting the approximate endocardium, midwall, and epicardium. The left ventricular region is divided into octants. **b:** Lagrangian circumferential strain evolution plots of points in the mid-wall for each octant for a breath-hold HARP-MRI sequence (dotted line), non-breath-hold HARP-MRI sequence (solid line), and standard 1-1 SPAMM sequence (dot-dashed line). The *y*-axis denotes the Lagrangian circumferential strain in percentage values, while the *x*-axis denotes time in milliseconds. **c:** Maximal Lagrangian circumferential shortening in the mid-wall (for the same volunteer as in **b**) computed by a breath-hold HARP-MRI sequence (Y1), non-breath-hold HARP-MRI sequence (Y2), and 1-1 SPAMM sequence (Y3). Solid lines with crosses at the ends show the range of the measured maximal shortening for all three methods in three volunteers. Dotted lines with dots at the ends show the range of the measured maximal shortening for the two HARP-MRI studies in six volunteers.

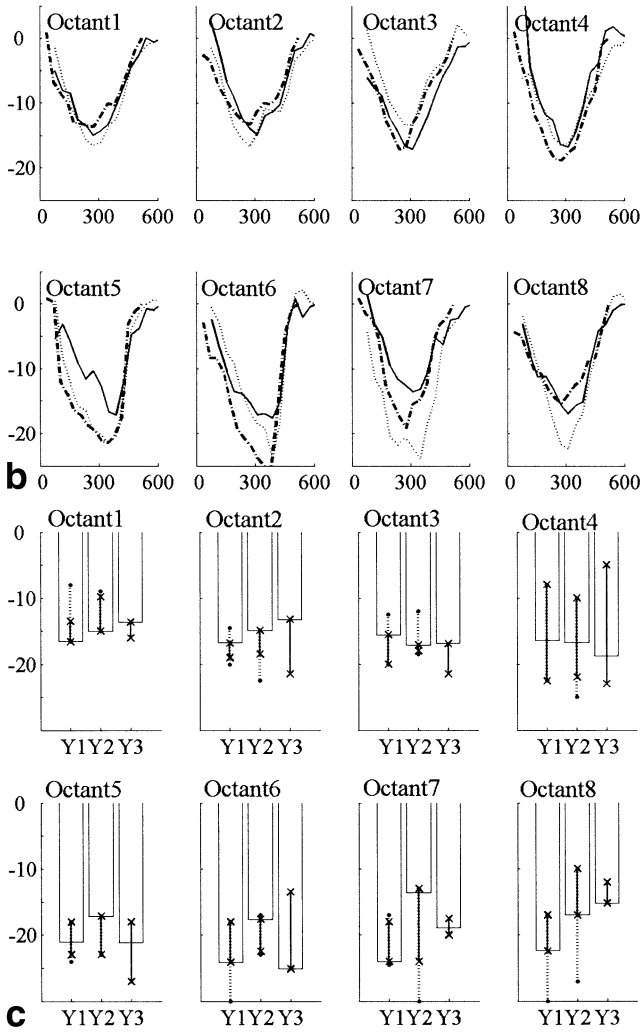

FIG. 6. Continued.

less of the origin of the tissue, were obtained by computing appropriate spatial derivatives of the HARP images (see Ref. 13 and Appendix A). For better visualization, images containing synthetic tags with Fourier series coefficients (3.0, 2.0, 1.0, and 0.0625) for the two tag directions were then computed (see Ref. 17 and Appendix B) and overlaid on the Eulerian strain maps. After definition of an approximately circular grid within the myocardium, plots of the time evolution of circumferential Lagrangian strain were computed in octants of the left ventricle (see Ref. 12 and Appendix A). Lagrangian strains were measured by computing the change in length between two points at the current frame over the original length at the reference time frame; i.e., the strain estimate follows a specific piece of tissue in time. Comparisons between the Lagrangian circumferential strains for the three methods were quantified using linear regression analysis and Bland-Altman plots.

RESULTS

Figure 4 shows the harmonic magnitude and HARP images (with a mask applied) of one volunteer and one tag direction. The data were obtained in a two-heartbeat breath-hold. Figure 4a and b are end-diastolic images (observe the relatively straight lines in the phase image), while Fig. 4c and d are end-systolic images (note the bending in the phase wrap lines in Fig. 4d).

Figure 5a–c shows Eulerian strain maps overlaid by synthetic tags, computed from the HARP images of one volunteer for the three different scans. The time series begins in early systole (34.6 ms) and ends in diastole (622.8 ms). All three sequences reveal a progressive increase in the circumferential shortening during systole that can be visualized by the bending of the tag lines and the increased dark blue coloration in the strain maps. The diastolic images show a gradual decrease in the circumferential shortening.

Next, the approximate subepicardial and subendocardial contours were defined on an end-systolic frame, from which the mid-ventricular contour was computed, and the myocardium was divided into octants (Fig. 6a). In each octant, 10 pairs of points located on the midwall, with a spacing of one-half of an octant between two points in a pair, were tracked using HARP tracking (12), and their Lagrangian circumferential strains were computed and averaged to reduce noise (see Appendix A).

Figure 6b shows the temporal evolution of the mid-wall Lagrangian strain in each of eight octants computed for the three acquisitions for one volunteer. These results are representative. The dotted line indicates a two-heartbeat breath-hold HARP-MRI sequence (Y1), the solid line represents a non-breath-hold HARP-MRI sequence (Y2), and the dot-dash line indicates a conventional double-breath-hold (12 heartbeats each) 1-1 SPAMM MR tagging sequence (Y3). Positive values indicate circumferential stretching, while negative values indicate circumferential shortening. From these plots, it is observed that all octants exhibit normal shortening. For octants 1–4, the trends of the three curves appear to be very similar. Octants 5–8 appear to be noisier, and there is a greater discrepancy between the three curves, especially at higher strain values. This could be because these octants are farther away from the phased-array coils and therefore have higher noise levels in the images themselves. Other factors, such as differences in breath-hold strategies, pulse sequences, and slice prescription, may also account for these discrepancies.

Figure 6c shows bar plots of the maximal shortening for eight octants in the same volunteer measured using all three methods. Dotted lines with dots on their ends show the range of maximal shortening measured for all six volunteers during the two HARP-MRI scans, while the solid lines with crosses on their ends show the range of maximal shortening measured using all three methods for three of the volunteers. From this plot, we see that in octants 1–5 there is a significant overlap in the ranges: the lower-limit difference is not more than 3%, and the upper-limit difference is not more than 4–5%. In octants 6–8, these differences are larger: the lower-limit difference is nearly 8%, and the upper-limit difference ranges between 3–7%. It is also observed from this plot that in these volunteers, the maximal shortening in the anterio-septal regions is lower than in the posterio-lateral regions.

Figure 7 quantitatively compares the Lagrangian circumferential strain (LCS) using linear regression analysis be-

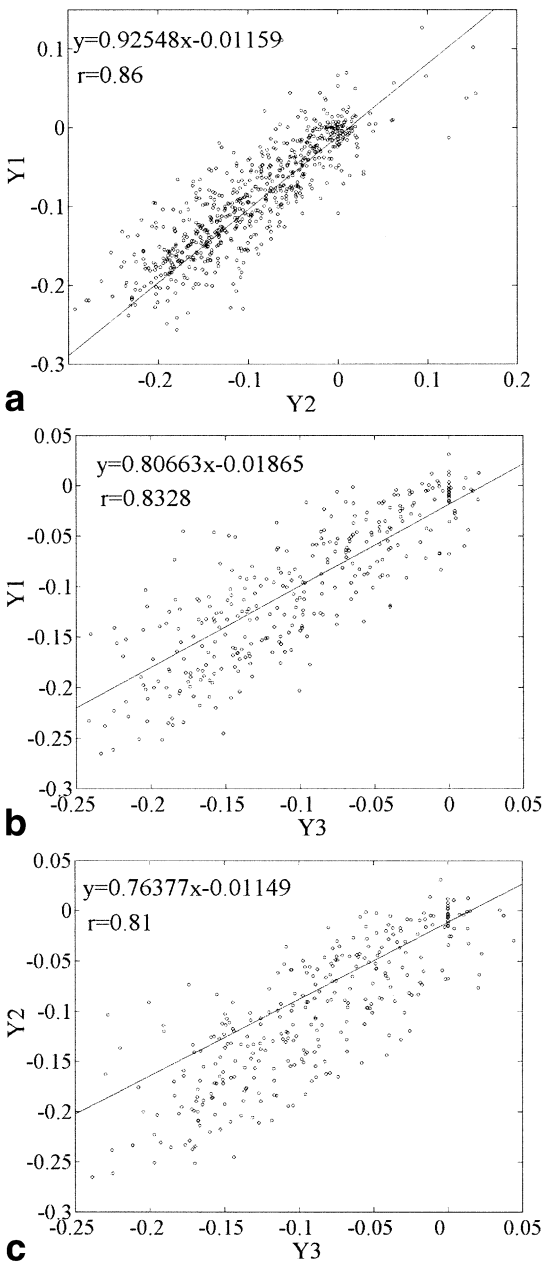

FIG. 7. Correlation between Lagrangian myocardial circumferential strains between (**a**) Y1 and Y2, (**b**) Y1 and Y3, and (**c**) Y2 and Y3. Y1 = breath-hold HARP-MRI, Y2 = non-breath-hold HARP-MRI, and Y3 = conventional 1-1 SPAMM tagging.

tween pairs of the three different scans. The correlation coefficients and the slopes in the linear regression plots for data obtained in all time frames were: 1) 0.86 and 0.92, respectively, between Y1 and Y2 (Fig. 7a) in all six volunteers; 2) 0.832 and 0.80, respectively, between Y1 and Y3 (Fig. 7b) in three volunteers; and 3) 0.81 and 0.76, respectively, between Y2 and Y3 (Fig. 7c) in three volunteers. While these values are reasonable, we observed higher correlation and slope values that were closer to unity between the two HARP-MRI methods than between each of the HARP-MRI methods and the conventional tagging method. Figure 8 shows Bland-Altman plots comparing the LCS between pairs of the three scans. The mean differences were -0.005 ± 0.037 (mean $\pm$ standard deviation (SD)) between Y1 and Y2 (Fig. 8a); 0.0142 ± 0.038 between Y1 and Y3 (Fig. 8b); and 0.013 ± 0.04 between Y2 and Y3 (Fig. 8c). These plots illustrate an increase in the mean value and SD in the Bland-Altman plots shown in Fig. 8b and c, in agreement with the results shown in Fig. 7.

To demonstrate the reliability of motion tracking in HARP-MRI images, several points in the myocardium were manually selected in the first time frame of one volunteer and then tracked in time. Figure 9 shows the tracked paths for each of these points using the three methods. The yellow dotted markers represent the selected points, and

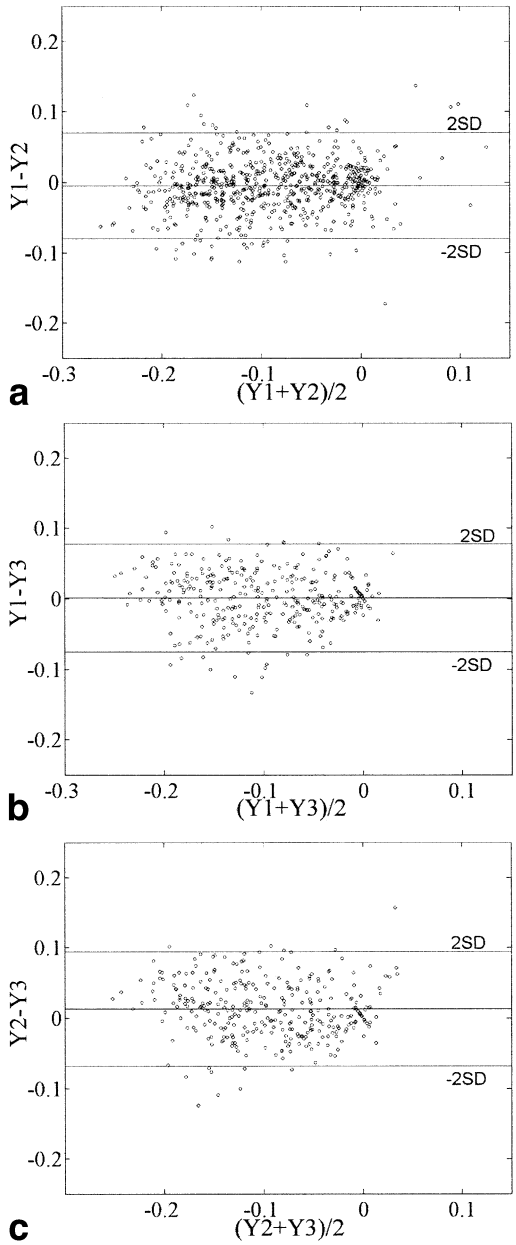

FIG. 8. Bland-Altman plots for the comparison of Lagrangian circumferential strains between (**a**) Y1 and Y2, (**b**) Y1 and Y3, and (**c**) Y2 and Y3. Y1 = breath-hold HARP-MRI, Y2 = non-breath-hold HARP-MRI, and Y3 = conventional 1-1 SPAMM tagging.

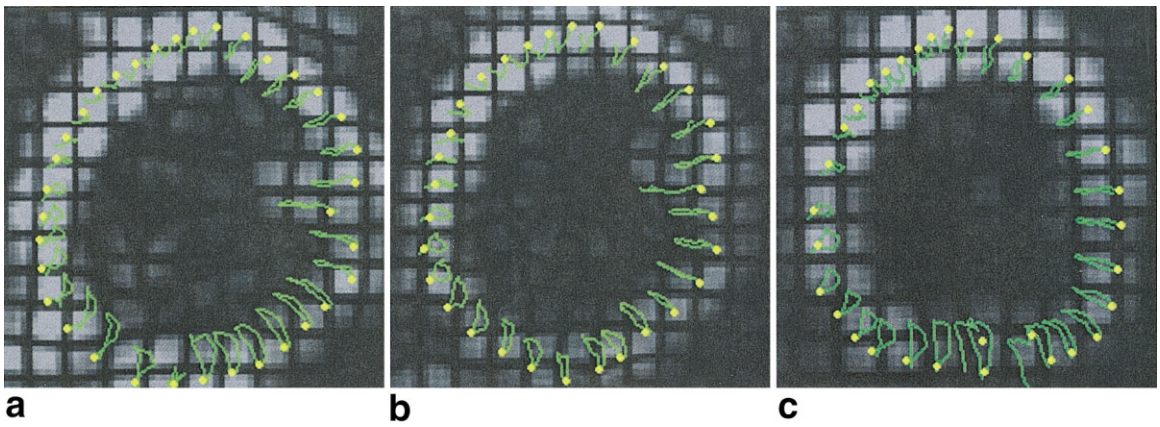

FIG. 9. Tracked paths of randomly selected points in the myocardium at end-diastole for: (**a**) breath-hold HARP-MRI, (**b**) non-breath-hold HARP-MRI, and (**c**) conventional breath-hold 1-1 SPAMM sequence.

the green colored lines depict the motion trajectories. From Fig. 9, it is observed that the trends in the tracked paths for all the three methods are similar.

DISCUSSION

The semi-automatic user-interface driven tag detection and strain visualization program—FINDTAGS—has been the gold-standard used in postprocessing tagged images (25,26). A validation of the strain measurements obtained from a conventional tagging sequence using HARP post-processing against FINDTAGS has already been presented (27). Accordingly, in this study we compared results obtained from the HARP-MRI sequence against those from a conventional tagging sequence. Both sequences were post-processed using HARP.

Figure 5 revealed that strain maps generated from HARP-MRI and from conventional tagging are qualitatively similar in appearance. The use of an optimized incrementing train of imaging flip angles preserves the SNR in the HARP-MRI images (20) over all cardiac frames, preventing its characteristic deterioration (results not shown, due to space considerations). In Fig. 5c, we notice an apparent brightening of the images due to the increased noise and interference from the DC peak at the later time frames. The conventional tagging pulse sequence could potentially be used with incrementing flip angles, but this feature is not presently available in our standard pulse sequence. We made the deliberate choice to demonstrate motion over only 60% of the cardiac cycle, in return for some additional signal per cardiac time frame, by allowing more longitudinal magnetization recovery at the end of each R-R interval.

The isolated yellow, orange, and red spots in Fig. 5 (especially at the two points where the right ventricle inserts into the left ventricle) could be falsely interpreted as diseased regions. Some of these artifacts become more apparent during later time frames, and we believe that they are due to the interference of the increasing DC peak with the harmonic peak. Applying a complementary SPAMM (CSPAMM) scheme (i.e., phase cycling of the second SPAMM tagging RF pulse) in combination with the HARP-MRI sequence should remove these artifacts (16). However, with CSPAMM, HARP-MRI would then take four heartbeats, instead of two, to acquire the images that are necessary to compute strain.

The strain evolution plots in Fig. 6b show that the HARP-MRI pulse sequence delivers trends and measurements of circumferential shortening, comparable to a conventional pulse sequence. Figures 8 and 9, however, reveal that there is greater similarity between the two HARP-MRI scans than between the HARP-MRI scans and the conventional tagging scans. Possible reasons for this difference include: 1) the sample size in the comparisons of the Y1 (or Y2) with Y3 was one-half that of the sample size in the comparisons between Y1 and Y2; 2) nonreproducibility in cardiac motion over several heartbeats; and 3) errors due to multicoil combinations using the FastHARP sequence. We note that the nonreproducibility of cardiac motion is most likely to negatively affect the conventional tagging sequence, because it requires 24 heartbeats to yield the required data. On the other hand, coil-combination problems will affect HARP-MRI exclusively, since conventional tagging typically acquires magnitude images. Despite these discrepancies, we believe that the results are encouraging and reasonable for the intended use of this sequence—to provide good qualitative strain measures in a cardiac stress-test protocol.

Real-time imaging using HARP-MRI images only one slice at a time. On each slice, 2D strain indices can be computed, and the relationship between these quantities and true 3D strain can be described mathematically (14). Although HARP-MRI can be programmed to cycle through a sequence of prescribed slices, there is no provision at present to acquire data sufficient for true 3D strain computations. However, a technique based on out-of-plane tagging and HARP (28) can be used in conjunction with HARP-MRI to obtain 3D strain information.

Ideally, slice motion in the out-of-plane direction is negligible, and the same slice is imaged every cardiac frame. In reality, the heart itself produces out-of-plane motion due to longitudinal shortening, and breathing and other subject motion can cause differences in the slice that is imaged. Although these issues could be directly addressed using navigator echoes and the slice-following technique (29) in conjunction with HARP-MRI, our pre-

liminary results indicate there is no obvious deterioration in the visual appearance or numerical trends in the strains created using HARP-MRI with breath-hold and non-breath-hold acquisitions. This makes a preliminary case for the use of HARP-MRI in monitoring myocardial function during stress tests with free breathing.

It was previously shown that standard tag-tracking methods (e.g., FINDTAGS) have accuracies better than the tag separation when there is a sufficiently high contrast-to-noise ratio (CNR). Similarly, HARP can measure tag displacements throughout the plane without restriction as to where the tag is, provided that the motion is spatially smooth (which is typical of normal heart motion). Under sudden or abrupt spatial changes in the strain pattern, as is the case with ischemic events, the use of a small acquisition box in *k*-space limits the dynamic range and resolution at which quantitative accuracy in strain measurements can be obtained. However, it has been shown that qualitative detection of ischemic regions whose dimensions are smaller than the tag separation is achievable (15,27).

To determine a more accurate quantification, however, one would need to use a higher-resolution sequence (5,6), which would require a much longer acquisition time.

In addition to the dynamic range, the speed of acquisition was another determining factor in the size of the *k*-space box imaged, as we desired to acquire adequate information to compute strain every 50 ms or better. Currently, our temporal resolution of 40 ms is close to standard temporal resolutions used in CINE cardiac MR images (~30–45 ms) (10). To improve the apparent temporal resolution of HARP-MRI, each echo train could be treated as a new piece of information, and the most recent four echo trains could be used to make one image every 10 ms using a sliding-window reconstruction technique. The effects of this procedure on strain computation should be investigated in the future. Finally, we note that with future optimization of the pulse sequence, it should be possible to acquire a 48 × 48 region in *k*-space while maintaining the same temporal resolution.

CONCLUSIONS

In this study the real-time acquisition of HARP images using the HARP-MRI pulse sequence was developed and demonstrated. Experimental results from six normal human volunteers depict 15–18 cardiac phases acquired over 60% of an R-R cycle with a time resolution of 40 ms. It was shown that postprocessing of the datasets acquired from just two adjacent heartbeats provides full quantification and visualization of 2D myocardial strain. An incrementing train of imaging RF flip angles was used to prevent rapid decay of the harmonic peaks, and thus provided high tag contrast over a large fraction of the cardiac cycle. It is hoped that the HARP-MRI sequence in combination with real-time analysis will be useful for clinical monitoring during dobutamine stress tests by providing a measure of myocardial function each heartbeat with a one-heartbeat delay.

APPENDIX A

From two harmonic images a_1 and a_2 with mutually perpendicular tag directions with tag frequencies o_1 and o_2, respectively, the Eulerian strain (difference in displacement between adjacent parts of the myocardium) is computed as follows (13,14):

$$\varepsilon_a(\mathbf{p},t;\mathbf{n}) = \frac{\|[\nabla^* \mathrm{a}\,(\mathbf{p},t)]^{-1}\,\mathbf{W}^{-T}\mathbf{n}\|}{\|\mathbf{n}\|} - 1$$

where

$$\mathrm{a}\,(\mathbf{p},t) = \begin{bmatrix} a_1\,(\mathbf{p},t) \\ a_2\,(\mathbf{p},t) \end{bmatrix},\ \mathbf{W} = \begin{bmatrix} \omega_1 \\ \omega_2 \end{bmatrix}^T.$$

n is the direction along which the Eulerian strain is computed, and the superscript T stands for the transpose of the vector or matrix.

The Lagrangian strain between two points $\mathbf{p_1}$ and $\mathbf{p_2}$ (change in length over unit length) is computed by first tracking the position of those two points in time. Since the phase of material points remains unchanged with time, the points are tracked to their new positions $\mathbf{y}(\mathbf{p_1})$ and $\mathbf{y}(\mathbf{p_2})$ by tracking their wrapped HARP. Now, the Lagrangian strain between the two points is given by (12):

$$\varepsilon(t;\mathbf{p}_1,\mathbf{p}_2) = \frac{\|\mathbf{y}(\mathbf{p}_1,t) - \mathbf{y}\,(\mathbf{p}_2,\,t)\|}{\|\mathbf{p}_1 - \mathbf{p}_2\|} - 1.$$

APPENDIX B

To produce crisp, sharp tag lines from a harmonic image, the following image is synthesized using the Fourier series expansion (17):

$$I_{synthetic} = c_0 D(\mathbf{p},\,t) + c_1 D(\mathbf{p},\,t)\sin(\phi(\mathbf{p},t)) + c_2 D(\mathbf{p},\,t)\cos(2\phi(\mathbf{p},\,t)) + c_3 D(\mathbf{p},\,t)\sin(3\phi(\mathbf{p},\,t))$$

where c_0, c_1, c_2, and c_3 are a set of coefficients that determine the sharpness of the tags.

REFERENCES

1. Zhu Y, Drangova M, Pelc NJ. Estimation of deformation gradient from cine-PC velocity data. IEEE Trans Med Imaging 1997;16;840–851.
2. Wedeen VJ. Magnetic resonance imaging of myocardial kinematics. Technique to detect, localize, and quantify the strain rates of the active human myocardium. Magn Reson Med 1992;27:52–67.
3. Zhu Y, Pelc NJ. Three-dimensional motion tracking with volumetric phase contrast CMR velocity imaging. J Magn Reson Imaging 1999;9; 111–118.
4. Reese TG, Feinberg DA, Dou J, Wedeen VJ. Phase contrast MRI of myocardial 3D strain by encoding contiguous slices in a single shot. Magn Reson Med 2002;47:665–676.
5. Aletras AH, Ding S, Balaban R, Wen H. DENSE: displacement encoding with stimulated echoes in cardiac functional MRI. J Magn Reson 1999; 137:247–252.
6. Aletras AH, Ding S, Balaban R, Wen H. High-resolution strain analysis of the human heart with Fast-DENSE. J Magn Reson 1999;140:41–57.
7. Zerhouni EA, Parish DM, Rogers WJ, Yang A, Shapiro EP. Human heart: tagging with MR imaging—a method for noninvasive assessment of myocardial motion. Radiology 1988;169:59–63.
8. Axel L, Dougherty L. MR imaging of motion with spatial modulation of magnetization. Radiology 1988;169:59–63.
9. Axel L, Dougherty L. Heart wall motion: improved method of spatial modulation of magnetization for MR imaging. Radiology 1989;171:841–845.

10. McVeigh ER, Atalar E. Cardiac tagging with breath-hold cine MRI. Magn Reson Med 1992;28:318–327.
11. Fischer SE, McKinnon GC, Scheidegger MB, Prins W, Meier D, Boesiger P. True myocardial motion tracking. Magn Reson Med 1994;31:401–413.
12. Osman NF, Kerwin WS, McVeigh ER, Prince JL. Cardiac motion tracking using CINE harmonic phase (HARP) magnetic resonance imaging. Magn Reson Med 1999;42:1048–1060.
13. Osman NF, Prince JL. Visualizing myocardial function using HARP MRI. Phys Med Biol 2000;45:1665–1682.
14. Osman NF, McVeigh ER, Prince JL. Imaging heart motion using harmonic phase MRI. IEEE Trans Med Imaging 2000;19:186–202.
15. Garot J, Bluemke D, Osman NF, Rochitte CE, Zerhouni EA, Prince JL, Lima JAC. Transmural contractile reserve after reperfused myocardial infarction in dogs. J Am Coll Cardiol 2000;36:2339–2346.
16. Kuijer JPA, Jansen E, Marcus JT, Rossum AC, Heethaar RM. Improved harmonic phase myocardial strain maps. Magn Reson Med 2001;46: 993–999.
17. Osman NF, Sampath S, Derbyshire JA, Atalar E, Prince JL. Synthetic tagged MR images for real-time HARP imaging. In: Proceedings of the 9th Annual Meeting of ISMRM, Glasgow, Scotland, 2001. p 829.
18. Sampath S, Derbyshire JA, Osman NF, Atalar E, Prince JL. Real-time imaging of cardiac strain using ultra FastHARP sequence. In: Proceedings of the 9th Annual Meeting of ISMRM, Glasgow, Scotland, 2001. p 111.
19. Fischer SE, McKinnon GC, Maier SE, Boesiger P. Improved myocardial tagging contrast. Magn Reson Med 1993;30:191–200.
20. Stuber M, Fischer SE, Scheidegger MB, Boesiger P. Toward high resolution myocardial tagging. Magn Reson Med 1999;41:639–643.
21. Bernstein MA, Grgic M, Brosnan TJ, Pelc NJ. Reconstructions of phase contrast, phased array multi coil data. Magn Reson Med 1994;32:330–334.
22. Wright RC, Riederer SJ, Farzaneh F, Rossman PJ, Yu L. Real-time MR fluoroscopic data acquisition and image reconstruction. Magn Reson Med 1989;12:407–415.
23. Hardy CJ, Darrow RD, Nieters EJ Roemer PB, Watkins RD, Adams WJ, Hattes NR, Maier JK. Real-time acquisition, display and interactive graphic control of NMR cardiac profiles and images. Magn Reson Med 1993;29:667–673.
24. Kerr AB, Pauly JM, Hu BS, Li KC, Hardy CJ, Meyer CH, Macovski A, Nishimura DG. Real-time interactive MRI on a conventional scanner. Magn Reson Med 1997;38:355–367.
25. Guttmann MA, Prince JL, McVeigh ER. Tag and contour detection in tagged MR images of the left ventricle. IEEE Trans Med Imaging 1994; 13:74–88.
26. Guttmann MA, Zerhouni EA, McVeigh ER. Analysis and visualization of cardiac function from MR images. IEEE Comput Graph Appl 1997; 17:30–38.
27. Garot J, Bluemke D, Osman NF, Rochitte CE, McVeigh ER, Zerhouni EA, Prince JL, Lima JAC. Fast determination of regional myocardial strain fields from tagged cardiac images using harmonic phase MRI. Circulation 2000;101:981–988.
28. Osman NF, Sampath S, Atalar E, Prince JL. Imaging longitudinal cardiac strain on short axis images using strain encoded imaging. Magn Reson Med 2001;46:234–334.
29. Stuber M, Spiegel MA, Fischer SE, Scheidegger MB, Danias PG, Pedersen EM, Boesiger P. Single breath-hold slice-following CSPAMM myocardial tagging. Magn Reson Mater Phys Biol Med 1999;9:85–91.